Biosensors and Bioelectronics 142 (2019) 111508

Contents lists available at ScienceDirect

Biosensors and Bioelectronics

journal homepage: www.elsevier.com/locate/bios

A laser-induced breakdown spectroscopy-integrated lateral flow strip (LIBS-LFS) sensor for rapid detection of pathogen

Jing Wu[a,1], Yong Liu[b,c,1], Youwei Cui[a], Xiaohui Zhao[b], Daming Dong[a,*]

[a] National Engineering Research Center of Intelligent Equipment for Agriculture, Beijing Academy of Agriculture and Forestry Sciences, Beijing, 100097, China
[b] Beijing Engineering Research Center for BioNanotechnology, CAS Key Laboratory for Biomedical Effects of Nanomaterials and Nanosafety, CAS Center for Excellence in Nanoscience, National Center for NanoScience and Technology, Beijing, 100190, China
[c] University of Chinese Academy of Sciences, Beijing, 100049, China

ARTICLE INFO

Keywords:
Lateral flow strip
Laser-induced breakdown spectroscopy
Pathogen detection
Ag_xAu_y bimetallic nanoparticles
Staphylococcus aureus

ABSTRACT

Incorporation of new readout methods with established analytical devices allows methodological innovations in analytical sciences. Herein, we present a new sensing platform by combining an ultrasensitive element analyzer, namely the laser-induced breakdown spectroscopy (LIBS) and a lateral flow strip (LFS). Ag_xAu_y bimetallic nanoparticles (Ag_xAu_yBNPs) are selected as the labels to deliver the optimal quantitative performance by analyzing the Ag (I) signal from the test (T) line of LFS. For prototypical application in pathogen detection, the LIBS-LFS sensor can achieve a detection limit of 1.6 cfu mL^{-1} of *Staphylococcus aureus* (*S. aureus*) within 10 min, which is superior to conventional methods. Importantly, the signals of Ag_xAu_yBNPs for visual and LIBS analysis are stable and still readable after the detection is finished and the test strip is stored for up to 13 days, suggesting a potential for long-term data preservation. This combination of LIBS with LFS provides a new concept toward integrated nano/analytical devices that can benefit various application scenarios.

1. Introduction

Recently, the lateral flow strip (LFS) technology has been extensively used for bioanalysis with advantages of simple operation, rapid processing, low-cost and long-term stability (Jaust-Rubio et al., 2018; Ren et al., 2019; Yang et al., 2019). Specifically, the Au nanoparticles (AuNPs)-incorporated LFS has been successfully transformed into an abundance of commercial products due to its eye-readability of the detection result. However, the status quo of commercial LFS products shows limited quantitative performances (Brangel et al., 2018; Coleman et al., 2019). To improve this situation, efforts have been oriented toward various labeling techniques that can collaborate with specific analytical instruments with high sensitivity. Alternative labels beyond AuNPs, including fluorescent materials (Deng et al., 2018a, b; He et al., 2018, Raman probes (Tran et al., 2019; Zhang et al., 2018), magnetic (Hu et al., 2019) or enzymatic NPs (Loynachan et al., 2018), and enzymes (Deng et al., 2018a, b), have been designed and coupled with a range of optical instruments for enhanced accuracy and sensitivity. These optical readout systems have shown good compatibility with LFS analysis due to their exemption of harsh sample pretreatment and prolonged detection time. Exploiting new LFS devices that are optically quantifiable is meaningful to further advance this technique toward quantitative applications.

Laser-induced breakdown spectroscopy (LIBS) is an atomic emission spectroscopy technique using highly energetic laser pulses to provoke optical excitation from the sample (Fu et al., 2018). After excitation, the created plasma light emissions can provide “spectral signatures” for element analysis. Compared to other techniques for element analysis such as mass spectroscopy, (Hu et al., 2018; Bendall et al., 2011; He et al., 2019; Pichaandi et al., 2019), LIBS has unique advantages for *in situ* quantification of trace elements such as pretreatment-free, high sensitivity, low sample consumption (1 μL), rapid processing (10 s), and flexibility in handling complex samples (water, soil, air and so forth) (Dong et al., 2017; Pardede et al., 2019; Yi et al., 2018). These superiorities make LIBS a robust partner for metal NPs-labeled immunosensors in quantitative scenarios. However, a prerequisite to apply LIBS in immunosensors is that the NPs-labeled immunocomplex must be homogeneously distributed around a surface to obtain repeatable and stable LIBS signals, which can be exceptionally difficult to realize. Thus, the feasibility of LIBS for immunosensors has been scarcely investigated. Recently, Markushin's group has applied LIBS for magnetic immunoassays using TiO_2 NPs as labels (Markushin et al.,

* Corresponding author.
E-mail addresses: dongdm@nercita.org.cn, damingdong@hotmail.com (D. Dong).
[1] These authors contributed equally to this work.

https://doi.org/10.1016/j.bios.2019.111508
Received 25 April 2019; Received in revised form 25 June 2019; Accepted 12 July 2019
Available online 13 July 2019
0956-5663/

2015). However, complex procedures of vacuum treatment are needed to ensure homogeneous distribution of the labeled samples, which impedes the use of this method in real-world settings.

In this contribution, we have developed a new sensing format by combining LIBS and LFS (LIBS-LFS). Homogeneous distribution of the NPs can be facilely achieved on the test (T) line of LFS thanks to the uniform coating of primary antibodies on the nitrocellulose (NC) membrane, which is critical for collecting stable LIBS signals. To evaluate the quantitative performances of this sensor, we perform the detection of *Staphylococcus aureus* (*S. aureus*) as a model application, which is a common pathogenic bacteria associated with food poisoning and human health (Rubab et al., 2018). Our method can be finished within 10 min and reach a detection limit of 1.6 cfu mL^{-1}, showing an effective collaboration of LIBS and LFS that is promising for rapid and accurate detection of trace targets in clinical diagnosis, food analysis, and environmental monitoring.

2. Material and methods

2.1. Material & instrumentation

Antibody for capture of *S. aureus* (Ab_1, 1.6 mg mL^{-1}, cataloged number: ab37644) was purchased from Abcam (UK). Antibody for label of *S. aureus* (Ab_2, 1.0 mg mL^{-1}, cataloged number: bs-0362r) was from Bioss (Beijing, China). The bovine serum albumin (BSA, cataloged number: A8020), goat anti mouse IgG (cataloged number: SPA131) and mouse IgG (cataloged number: SP031) were from Solarbio (Beijing, China). The microorganisms we used including *S. aureus*, Bacillus subtilis (*B. subtilis*), *Klebsiella pneumoniae* (*K. p.*) and *Escherichia coli* (*E. coli*) were obtained from Beijing Lablead Co. Ltd. (Beijing, China). Chloroauric acid ($HAuCl_4.3H_2O$, cataloged number: 16903-35-8), ferric chloride ($FeCl_3.6H_2O$, cataloged number: 10025-77-1), copper sulfate ($CuSO_4$, cataloged number: 7758-98-7) were from Beijing Chemical Works (Beijing, China). $AgNO_3$ (cataloged number: s116266) and trisodium citrate (cataloged number: s116311) were obtained from Aladdin (Shanghai, China). Tablets of phosphates used to prepare 0.01 M phosphate-buffered saline (PBS, pH 7.4, cataloged number: P1000) and Tween-20 (cataloged number: T8220) were from Solarbio (Beijing, China). The nitrocellulose (NC) membrane was from Startorius (Germany, cataloged number: CN140). The polyvinyl chloride (PVC) sheet, the sample pad (cataloged number: SB08) and the absorbent pad (cataloged number: SX27) were from Shanghai Kinbio Technology Co. Ltd (Shanghai, China). The Fe_3O_4 nanoparticles (Fe_3O_4 NPs, 5 mg mL^{-1}, 30 nm, cataloged number: 060115) were from Ocean Nanotech (USA). The powder of CuO nanoparticles (CuO NPs, 50 nm, cataloged number: DXN-KD50) was from Nantong Darcy Nano Technology Co., Ltd (Nantong, China). The water was deionized and ultrafiltered using a Milli-Q apparatus.

We employed transmission electron microscopy (TEM, SU-8220, Hitachi, Japan), dynamic light scattering analyzer (DLS, EV370X, Horiba, Japan) and ultraviolet–visible spectrometer (UV–vis, Shimadzu, UV-2600) for the characterization of Ag_xAu_y bimetallic nanoparticles (Ag_xAu_yBNPs, x:y is the mass ratio of Ag to Au). We also employed the inductively coupled plasma (ICP, Teledyne Leeman Labs Prodigy 7) to detect the concentration of metal element in NPs.

The LIBS system includes a laser, a spectrometer, a high-precision three-dimensional platform and a digital signal delay generator (Scheme 1A). The laser of Q-switched Nd:YAG (1064 nm, CFR200, Quantel Ltd., Les Ulis, France) is used to excite plasma of samples by focusing on sample surface with lens. The spectrometer (HR2000+, Ocean Optics Co. Ltd., USA) with an optical fiber is to collect and analyze the signal of laser-induced plasma. The high-precision three-dimensional platform is to carry and adjust the analysis position of sample by a stepper motor. The digital signal delay generator is used to generate a trigger delay between spectrometer acquisition and the laser. With the laser, spectrometer, sample platform and digital signal delay generator, the LIBS could precisely ionize and detect trace samples in a few seconds.

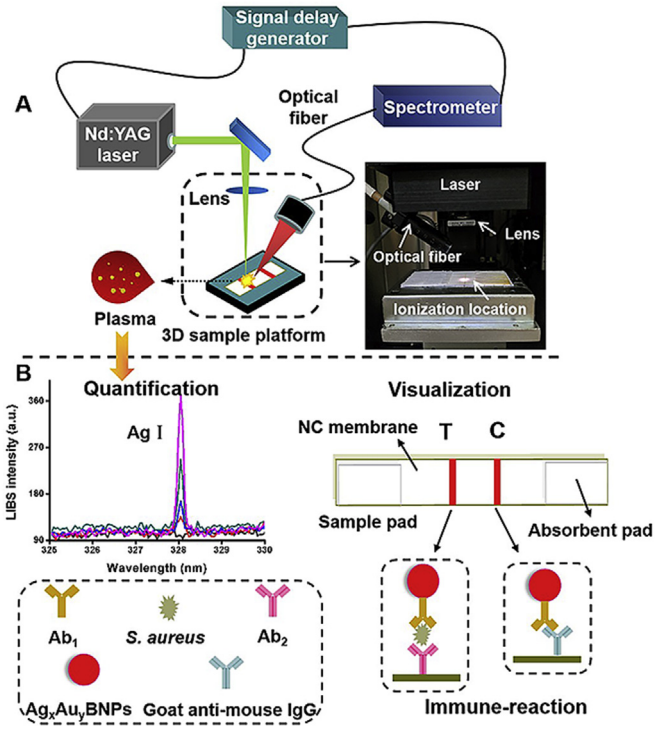

Scheme 1. Schematic illustration of the LIBS-LFS sensor for *S. aureus* analysis. (A) Schematic diagram of the LIBS system for element analysis on LFS. The LIBS system includes a laser, a spectrometer, a high-precision three-dimensional platform and a digital signal delay generator. The photograph shows the real intact LIBS for element analysis. (B) Principle of the LIBS-LFS sensor for *S. aureus* analysis, including the immune-reaction on NC membrane, the visualization by the naked eye and the spectroscopic quantification by LIBS. The visual readout for *S. aureus* analysis is based on the color change on T line of LFS. The spectroscopic quantification for *S. aureus* analysis is based on the LIBS analysis of Ag (I) on the T line.

2.2. Synthesis of Ag_xAu_yBNPs

Ag_xAu_yBNPs were prepared according to the literature (Hostetler et al., 1998). Briefly, we heat 100 mL of soultion containing 1.4 mL of trisodium citrate solution (1%, mass fraction) to boil under reflux with stirring. Further, to add 1.0 mL of the mixture solution of $AgNO_3$ and $HAuCl_4$ (the mass ratios of Ag to Au: 4:1, 3:2, 1:1, 2:3, and 1:4) to the previous solution and keep heating for 15 min. After cooling, we collected the prepared solution and stored it at 4 °C for further use. The processes of synthesis of AgNPs and AuNPs were similar to that of Ag_xAu_yBNPs. 1.0 mL of $AgNO_3$ solution and $HAuCl_4$ (0.01%, mass fraction) were used for synthesis of AgNPs and AuNPs, respectively.

2.3. Preparation of Ag_xAu_yBNPs-Ab

The conjugates of Ag_xAu_yBNPs-Ab were prepared according to our previous work (Deng et al., 2018a, b). Firstly, we adjusted the pH of the Ag_xAu_yBNPs solution to 8.5 using 0.2 M of K_2CO_3 solution. Next, we added Ab (25 μg mL^{-1}) to the previous solution and stirred for 20 min for synthesis of Ag_xAu_yBNPs-Ab. Then, we used BSA solution (1%, mass fraction) to block the residual sites on the surface of Ag_xAu_yBNPs-Ab for 5 min. Finally, after centrifuging the mixture for twice (9500 rpm, 30 min), we suspended the conjugates of Ag_xAu_yBNPs-Ab in the developing solution and stored them at 4 °C for further use.

2.4. Fabrication of LFS

The LFS consists of four components: sample pad, NC membrane, absorbent pad, PVC sheet. Firstly, we dispensed Ab_2 (1.0 mg mL^{-1}) and goat anti-mouse IgG (0.5 mg mL^{-1}) onto the surface of NC membrane with a dispenser to form the lines of Test (T) and Control (C), following by drying it at 37 °C for 1 h. Then, we assembled sample pad, NC membrane with T and C line, and absorbent pad onto the surface of PVC sheet. Finally, to cut the assembled PVC sheets into strips with a width of 4 mm and store them at 4 °C for future use.

2.5. Microorganism culture

All the strains (S. *aureus*, *B. subtilis*, *K. p.*, and *E. coli*) were cultured and maintained in 500 mL of nutrient broth at 37 °C with shaking for 48 h. The strains were harvested by centrifugation (5000 rpm, 20 min) and washed for three times by sterilized phosphate-buffered saline (PBS, 10 mM phosphate and 150 mM NaCl). Then, the bacteria were suspended in 50 mL of PBS solution for further use. The bacteria number [number of colony-forming units per milliliter (cfu mL^{-1})] was determined by conventional plate counting method.

2.6. Procedure of LIBS-LFS sensor for S. aureus analysis

For *S. aureus* analysis, we firstly added the mixture of *S. aureus* (50 μL) and Ag_xAu_yBNPs-Ab_1 (50 μL) to the sample pad, following by washing the strip with PBST and drying for 5 min. We then applied the LIBS for analysis of the signal of Ag_xAu_yBNPs on T line of the previous strip. After placing the strip on the sample platform of LIBS, we adjusted the lens and the location of platform to choose the analysis position of T line of strip. We then used the laser with the optimal operational parameters (200 mJ of laser energy, 75 μm of spot size and no delay time) to excite the plasma of samples, following by collecting the emission spectrum of Ag_xAu_yBNPs with the spectrometer. Before the experiment, a background spectrum was collected by the spectrometer. Finally, based on the characteristic peak of Ag, we constructed the correlation of the LIBS intensity of Ag on T line of strip and the concentration of *S. aureus* for quantitative analysis.

3. Results and discussion

3.1. Design and feasibility of LIBS-LFS sensor for S. aureus analysis

The principle of the LIBS-LFS sensor includes two parts: the visual analysis based on the color change on LFS (similar to conventional LFS), and the spectroscopic analysis using LIBS (Scheme 1B). Ag_xAu_y bimetallic nanoparticles (Ag_xAu_yBNPs, x:y represents the mass ratio of Ag/Au) are selected as the signal generator for LIBS detection whose optimization will be discussed later. The immunoreaction between Ag_xAu_yBNPs-Ab_1 (capture antibody, Ab_1), *S. aureus* and Ab_2 (label antibody, Ab_2) results in the accumulation of Ag_xAu_yBNPs on the T line of LFS, which not only gives a visually readable signal, but also can be analyzed by LIBS in a few seconds for quantitative analysis of *S. aureus*. The combination of excess Ag_xAu_yBNPs-Ab_1 and goat anti-mouse IgG on the control (C) line ensures the validity of the LFS detection. The LFS can be directly subjected to LIBS analysis without any pretreatment, in which the Ag and Au elements in Ag_xAu_yBNPs are ionized and the signal intensity of Ag (I) (the peak at 328.0 nm) is chosen for quantitative analysis due to its higher sensitivity compared to Au (I) (the peak at 242.7 nm) (Fig. 1A and B). This direct analysis of trace Ag element on the T line of LFS enables rapid and sensitive detection of *S. aureus* in 10 min, which is a reasonable time consumption for LFS detection.

Some recent works have applied LIBS for pathogen detection by analyzing endogenous elements originally from the pathogen, which suffers from diminished specificity compared to immune-based methods (Gaudiuso et al., 2019; Liao et al., 2019). We thus investigated the feasibility of LIBS-LFS sensor for *S. aureus* analysis using antibody-conjugated AuNPs as the label (Fig. S1). After introducing different concentrations of *S. aureus* and incubating for 10 min, the strip can be both visually read by the naked eye (Fig. S1A) and quantitatively analyzed by LIBS (Fig. S1B). The signal intensity of Au (I) increased progressively (from 44.2 to 95.2) with the increasing concentration of *S. aureus* (from 0 to 10^7 cfu mL^{-1}), while there was no observable Au signal on T line of the negative control strip. These results confirmed that LIBS could be directly applied in quantitative analysis of *S. aureus* on LFS, which was the foundation of our LIBS-LFS sensor.

3.2. Selection and characterization of nanomaterial labels for LIBS-LFS sensor

We anticipated that the LIBS-LFS sensor should provide sensitive signals for both visual and spectroscopic analysis, which can be optimized by tuning the composition of the nanoparticle labels. Hence, we first compared the detection sensitivity of LIBS to different metal elements in both ion (Au^{3+}, Ag^{+}, Cu^{2+}, and Fe^{3+}) and nanoparticle states (AuNPs, AgNPs, CuO NPs, and Fe_3O_4 NPs). The measured characteristic peaks of these four elements (Au (I), Ag (I), Cu (I), and Fe (II)) were 242.7, 328.0, 324.7, and 238.1 nm, respectively (Fig. S2). We selected NPs with similar sizes for use to minimize the interference of particle size in LIBS sensing. As characterized by dynamic light scattering analyzer (DLS), the hydrodynamic sizes of AuNPs, AgNPs, CuO NPs, and Fe_3O_4 NPs were 28.2, 43.8, 50.7, and 32.7 nm (Fig. S3). Under both the ion and nanoparticle state, the LIBS intensities of Au (I), Ag (I), Cu (I), and Fe (II) increased in accord with increased concentrations of the metal elements (Fig. 1A and B). However, the signal intensity of Ag (I) showed the highest sensitivity to the variation of metal concentration, indicating an optimal quantitative performance by using Ag (I) to label the LIBS-LFS sensor.

We also optimized the labeling material for the visual readout of the LIBS-LFS sensor. To compromise the performance of visual and LIBS readout, we proposed that alloyed materials of Ag and Au can deliver the optimal result. Thus, we synthesized Ag_xAu_yBNPs with designed combinations of Ag and Au at the Ag/Au mass ratios of 1:4, 2:3, 1:1, 3:2, and 4:1 to label the target since AgNPs showed lower sensitivity in visual readout than AuNPs (Fig. 1C). ICP measurements showed that the Ag/Au mass ratios of the prepared Ag_xAu_yBNPs were 1:6.2, 2:4.6, 1:0.8, 3:1.6, and 4:0.6, respectively, which were close to the expected values (Table S1). These NPs exhibited different colors and were endowed with similar particle sizes as confirmed by transmission electron microscopy (TEM) and DLS (Fig. S4, Fig. S5 and Table S1). To simplify the optimization procedure and reduce the cost, we used different volumes of Ag_xAu_yBNPs-Ab (mouse IgG) to react with the goat anti mouse IgG on C line and compared the visual sensitivity of different Ag/Au combinations. The visual detection result of Ag_3Au_2BNPs was superior to other combinations including pure AuNPs (Fig. 1C), which also showed comparable LIBS intensity of Ag (Fig. 1D) and Au (Fig. 1E). For LIBS analysis, the spot size of 75 μm was chosen as the optimal condition (Fig. S6). We thus chose Ag_3Au_2BNPs as the optimal labels for the LIBS-LFS sensor.

We characterized Ag_3Au_2BNPs before applying them in LIBS-LFS analysis using TEM, the LIBS analyzer, ultraviolet–visible (UV–vis) spectroscopy and DLS measurement (Fig. 2). The sizes of Ag_3Au_2BNPs were ~30–40 nm as characterized by TEM (Fig. 2A), which corresponded well with the DLS result (32.67 nm, Fig. 2B). The signals of Au (I) and Ag (I) in the LIBS spectrum were consistent with the composition of Ag_3Au_2BNPs (Fig. 2C). After incubation with Ab, Ag_3Au_2BNPs displayed an absorbance peak at 280 nm, which matched well with the characteristic peak of protein antibodies (Fig. 2D). This indicated that Ab was successfully labeled onto the surface of Ag_3Au_2BNPs. Meanwhile, the size of Ag_3Au_2BNPs-Ab grown to 50.75 nm compared to bare Ag_3Au_2BNPs. TEM images also confirmed the affinity of Ag_3Au_2BNPs-Ab to the surface antigen of *S. aureus*, in which a large quantity of NPs

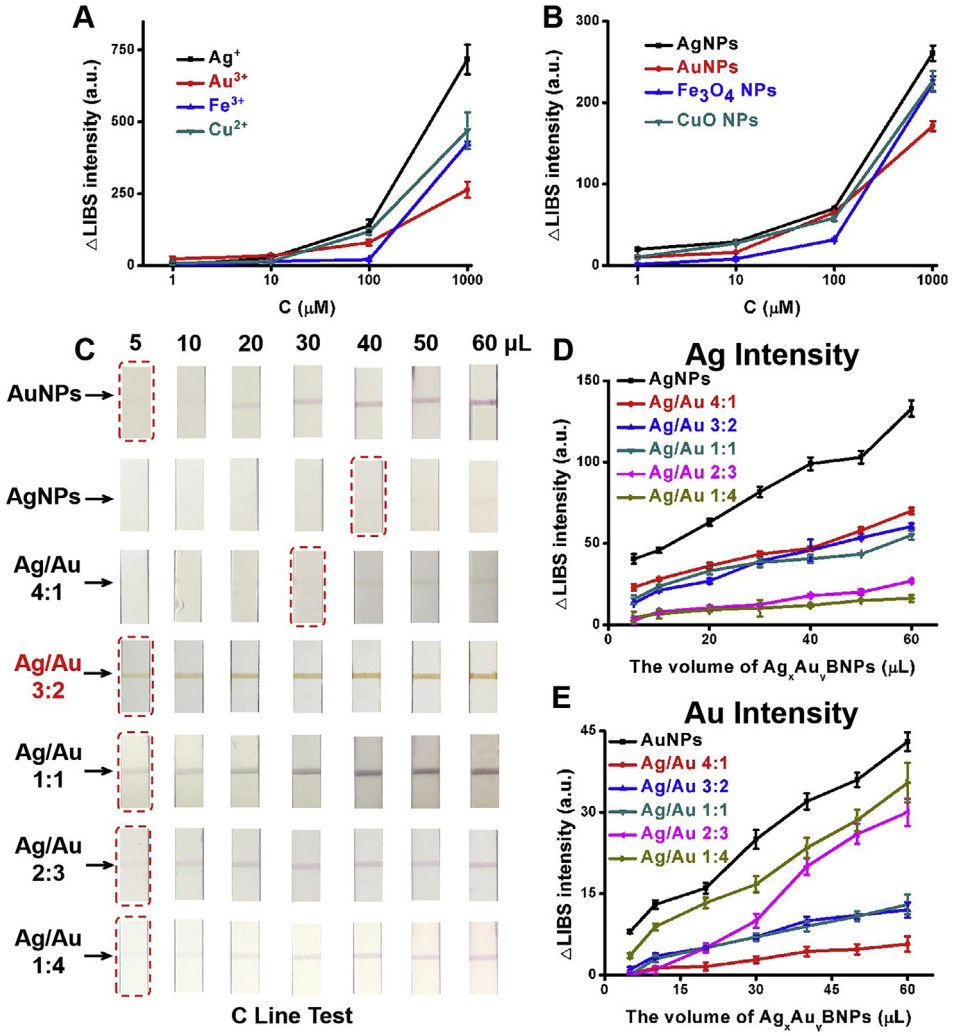

Fig. 1. The selection of labels for LIBS-LFS sensor. (A) and (B) The sensitivity of LIBS for analysis of different elements in ions ($AgNO_3$, $HAuCl_4$, $FeCl_3$, and $CuSO_4$) and NPs (AgNPs, AuNPs, Fe_3O_4 NPs, and CuO NPs) from 1 to 1000 μM. The concentrations of Ag, Au, Fe and Cu in NPs are determined by ICP. (C) The comparison of visual sensitivities of LFS using different NPs (AuNPs, AgNPs, and Ag_xAu_yBNPs with different mass ratios of Ag/Au) as labels. Different volumes (5–60 μL) of NPs-Ab (mouse IgG) are used to react with the goat anti-mouse IgG on C lines. (D) and (E) The LIBS analysis of Ag and Au on C lines with different volumes of probes, respectively. △LIBS intensity represents the intensity of sample minus that of blank sample. The error bars represent the standard deviation from three replicates (n = 3).

were observable on the cell wall of *S. aureus* (Fig. 2E and F). Summarily, these characterizations suggested that the Ag_3Au_2BNPs and Ag_3Au_2BNPs-Ab were successfully prepared and could be effectively employed for LIBS-LFS detection of *S. aureus*.

3.3. Sensitivity of LIBS-LFS sensor for S. aureus analysis

We investigated the sensitivity of the LIBS-LFS sensor for *S. aureus* analysis (Fig. 3). The brownish color of T lines on the strip gradually deepened with the increasing concentration of *S. aureus* from 0 to

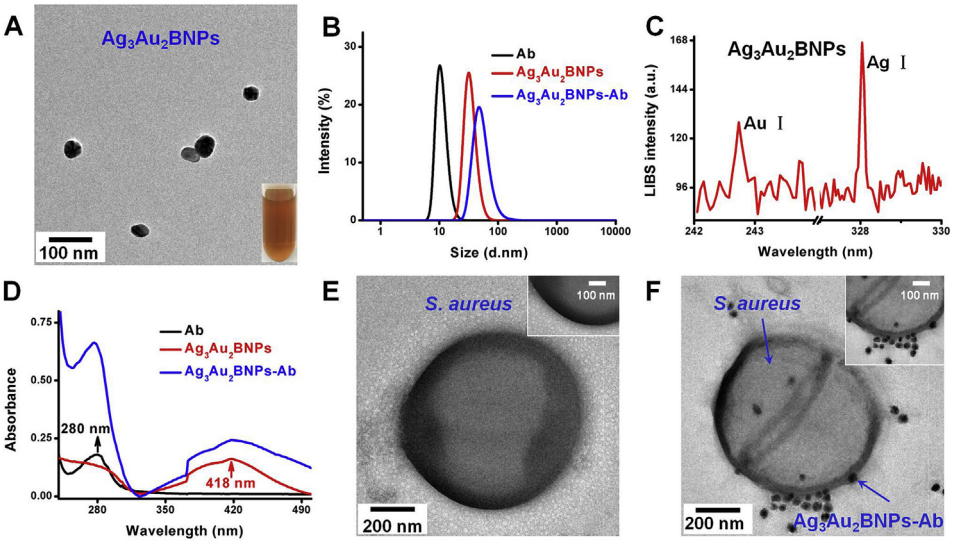

Fig. 2. Characterizations of Ag_3Au_2BNPs and Ag_3Au_2BNPs-Ab. (A) TEM image of Ag_3Au_2BNPs. The inset is the photographic image of Ag_3Au_2BNPs solution. (B) DLS measurement of Ag_3Au_2BNPs and Ag_3Au_2BNPs-Ab. (C) LIBS spectrum of Ag (I) and Au (I) in Ag_3Au_2BNPs. (D) UV–Vis spectra of Ag_3Au_2BNPs and Ag_3Au_2BNPs-Ab. (E) and (F) TEM images of *S. aureus* and the immunocomplex of Ag_3Au_2BNPs-Ab-*S. aureus*. The insets in (E) and (F) are the high magnification TEM images of these samples.

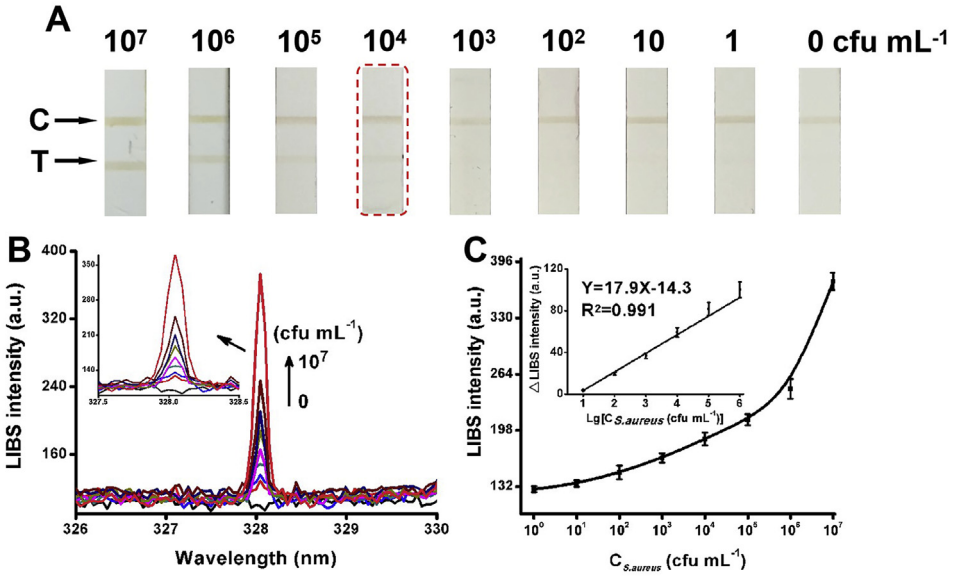

Fig. 3. Sensitivity of the LIBS-LFS sensor for *S. aureus* detection. (A) Photographic images of LFS for *S. aureus* analysis with different concentrations (0-10^7 cfu mL^{-1}). (B) Averaged LIBS spectra of T lines for different concentrations of *S. aureus*. The inset shows the enlarged spectra for *S. aureus* analysis. (C) The corresponding calibration curve (1 to 10^7 cfu mL^{-1}) and the range of linear detection for *S. aureus* (10 to 10^6 cfu mL^{-1}) in the inset. △LIBS intensity in the inset represents the intensity of sample minus that of blank sample. The error bars represent the standard deviation from three replicates (n = 3).

10^7 cfu mL^{-1}, delivering a visible detection limit of 10^4 cfu mL^{-1} (Fig. 3A). The LIBS intensity (the intensity of sample, Y) of Ag (I) at 328.0 nm increased progressively with the concentration of *S. aureus* ($C_{S.\ aureus}$ (cfu mL^{-1}, X) increasing from 0 to 10^7 cfu mL^{-1} (Fig. 3B and C), giving a linear correlation (Y = 17.9X-14.3, R^2 = 0.991) in the range of 10 to 10^6 cfu mL^{-1} (Inset of Fig. 3C). To eliminate the impact of random error, we used △LIBS intensity (the intensity of sample minus that of blank sample) versus Lg [$C_{S.\ aureus}$ (cfu mL^{-1})] to construct the calibration curve. The limit of detection (LOD) of the LIBS-LFS sensor was estimated to be 1.6 cfu mL^{-1}, which was defined as 3S/M (S = 4.7, M = 8.7, where S was the value of the standard deviation of the blank sample and M was the slope of the standard curve within the linear range of the low concentrations). This LOD was acceptable for several standards of *S. aureus analysis* in food samples (10^3 cfu g^{-1} of China (GB 29921–2013) and 10^4 cfu mL^{-1} of USA, Australia and New Zealand (Yu et al., 2016)). Thus, the sensitivity of FLS was significantly enhanced by integrating with the LIBS analyzer. These results also indicated that the dynamic detection range of our LIBS-LFS sensor was tunable from 10^4–10^7 cfu mL^{-1} to 10–10^6 cfu mL^{-1} simply by switching the readout method.

We compared the analytical performances of the LIBS-LFS sensor with other sensing platforms for *S. aureus* detection in terms of the sensitivity, detection range and time consumption (Table S2). Compared to the laser desorption/ionization mass spectrometry (LD/Ion-MS) (Lai et al., 2015), our method exhibited improved sensitivity and reduced time consumption. Besides rapid processing, the sensitivity of the LIBS-LFS sensor has shown a ~6 to 180-fold increase compared to most of other techniques (chemiluminescent analysis (Fan et al., 2019), electrochemical analysis (Bhardwaj et al., 2017), surface plasmon resonance (SPR) (Verdoot et al., 2017), surface-enhanced Raman scattering (SERS) (Yuan et al., 2018) and colorimetric assay (Wang et al., 2017). The detection range of our method was comparable with others, indicating that the proposed sensor could meet the requirement of current diagnosis. The ultralow LOD of the LIBS-LFS sensor was not so necessary for our model target because it was excessively lower than the minimum permissible quantity of *S. aureus* in real samples. However, the extendibility of this method to other targets promised a useful platform for timely diagnosis.

3.4. Reproducibility, specificity and stability of the LIBS-LFS sensor

To ensure the signal reproducibility, five different laser spots on the T line were chosen to yield an average LIBS signal for one single test strip. The standard deviations (4.28%, 4.99%, 3.63%, 4.62%, and 4.73%) of five measurements on each T line of five strips indicated an acceptable distribution of AgAuBNPs in the detection region. To study the batch-to-batch variation, we applied the LIBS-LFS sensor for *S. aureus* analysis (10^8 cfu mL^{-1}) using five test strips in parallel (Fig. 4A and B). Negligible difference was found in the color of the five T lines (Fig. 4A). Besides, the corresponding LIBS intensities of the five tests showed a low variation of 3.16% relative standard deviation (RSD) (Fig. 4B). Together, the LIBS-LFS sensor possessed favorable reproducibility for pathogen detection.

We studied the specificity of our method for the detection of *S. aureus* (10^8 cfu mL^{-1}) (Fig. 4C and D). We evaluated the response of the LIBS-LFS sensor to other strains of bacteria including Bacillus subtilis (*B. subtilis*), *Klebsiella pneumoniae* (*K. p.*) and *Escherichia coli* (*E. coli*) with the same concentration, using PBS solution as the blank control. The colorimetric results showed that only the sample containing *S. aureus* produced positive signal (Fig. 4C). Moreover, the LIBS intensities of the interference groups (112.6, 117.8 and 115.4) were similar to that of the blank control (119.3) and obviously lower than that of the positive sample (328.2) (Fig. 4D). Thus, both the visual and LIBS analysis indicated the high specificity of the LIBS-LFS sensor for the detection of *S. aureus*.

Besides the reproducibility and specificity, we investigated the potential of the LIBS-LFS sensor for long-term data preservation (Fig. S7). The visual result and LIBS analysis of a single test strip were tested every other day during 13 days. After LIBS analysis, the brownish color on the ionized position of LFS slightly faded compared to the untested region (Fig. S7A). However, there was negligible color change in the untested positions on the strip throughout the 13 days. No obvious decay was observed for the LIBS intensity during preservation, showing an acceptable RSD of 2.34% (Fig. S7B). The signal stability of our sensor was advantageous for reliable tracking and comparison of the detection results throughout desired time points of diagnosis.

3.5. Detection of S. aureus in spiked samples

We further applied the LIBS-LFS sensor to detect *S. aureus* in spiked samples of drinking water, milk and orange juice (Table 1). The reference concentrations of *S. aureus* in spiked samples were determined by the plate counting method. Compared to the results of plate counting, the recovery rates of LIBS-LFS ranged from 90.1 to 111%, and the coefficient of variations (CV) were smaller than 10.6%. The agreement results between the LIBS-LFS sensor and plate counting

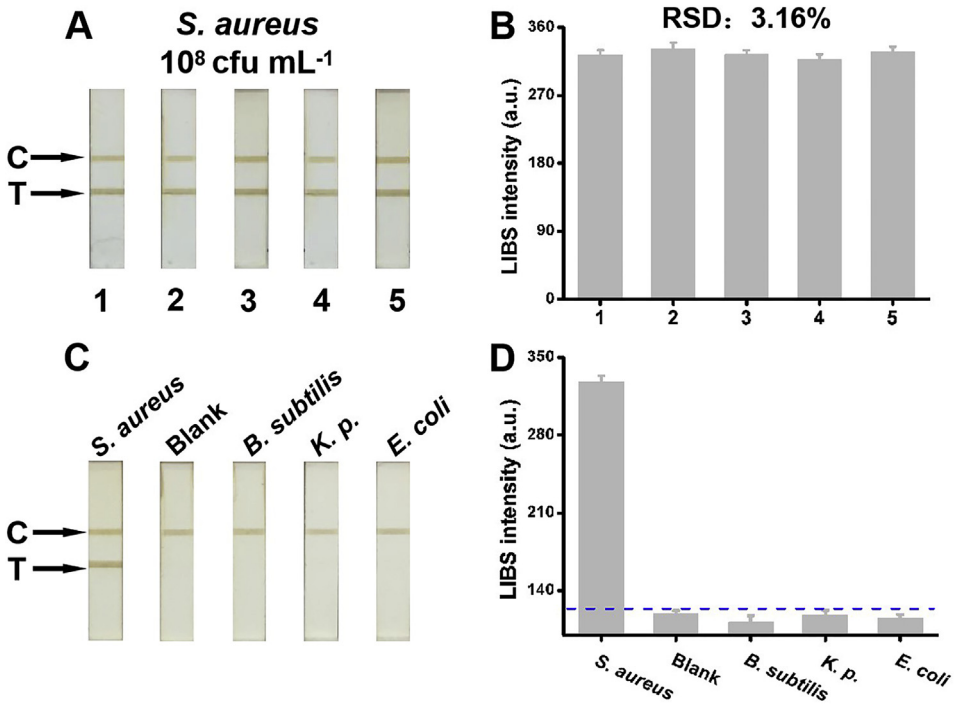

Fig. 4. (A) and (B) The reproducibility of LIBS-LFS sensor for *S. aureus* analysis. (A) Photographic images of LFS and (B) the LIBS analysis of five tests for *S. aureus* detection (10^8 cfu mL^{-1}). The RSD is calculated based on the five tests by LIBS. Error bars indicate the standard deviations of five measurements for each T line of strip. (C) and (D) The specificity of LIBS-LFS sensor for *S. aureus* analysis. (C) Photographic images of LFS and (D) the LIBS analysis of T lines of LFS for analysis of *S. aureus* (10^8 cfu mL^{-1}) and other interferences, using PBS solution as the blank control. The blue dash line represents the LIBS value of blank sample. (For interpretation of the references to color in this figure legend, the reader is referred to the Web version of this article.)

Table 1
Determination of *S. aureus* in spiked samples by LIBS-LFS sensor and plate counting method.

	Plate counting (10^3 cfu mL^{-1})	LIBS- LFS method (10^3 cfu mL^{-1})	Recovery (%)	CV(%)
Drinking water	2.22 ± 0.262	2.45 ± 0.230	110	10.4
	27.6 ± 5.15	29.5 ± 2.58	107	6.88
	439 ± 56.5	485 ± 31.4	110	10.5
Milk	4.84 ± 0.900	4.50 ± 0.696	93.0	7.02
	64.4 ± 6.03	71.2 ± 8.94	111	10.6
	418 ± 24.9	387 ± 30.9	92.6	7.42
Orange juice	5.86 ± 0.764	5.28 ± 0.266	90.1	9.90
	68.7 ± 6.23	74.4 ± 5.52	108	8.30
	703 ± 94.5	773 ± 68.4	110	9.96

method indicated that our method is extendable to practical applications.

4. Conclusions

In conclusion, a new and effective combination of LIBS and LFS is proposed to realize improved quantitative performance of conventional LFS sensors. The LIBS-LFS sensor is rapid, pretreatment free, and sensitive, and allows long-term data preservation and repeated readout. Despite the favorable results of the model application in pathogen analysis, this concept is still in the preliminary stage and remains to be further optimized and extended to other scenarios. Efforts are highly anticipated to miniaturize the LIBS reader to achieve improved portability of this integrated sensor. Besides, the performance of this platform in multichannel sensing of disease-relevant biomarkers is also under evaluation.

Declaration of competing interest

The authors declare that they have no known competing financial interests or personal relationships that could have appeared to influence the work reported in this paper.

CRediT authorship contribution statement

Jing Wu: Formal analysis, Data curation, Writing - original draft. **Yong Liu:** Writing - review & editing. **Youwei Cui:** Formal analysis. **Xiaohui Zhao:** Investigation. **Daming Dong:** Investigation, Methodology, Conceptualization.Acknowledgements

This work was supported by National Natural Science Foundation of China [31622040, 31600417], and Distinguished Scientist Development Program of Beijing Academy of Agriculture and Forestry Sciences [JKZX201904].

Conflict of interest

The authors declare no conflicts of interest.

Appendix A. Supplementary data

Supplementary data to this article can be found online at https://doi.org/10.1016/j.bios.2019.111508.

References

Bendall, S.C., Simonds, E.F., Qiu, P., Amir, E.A.D., Krutzik, P.O., Finck, R., Bruggner, R.V., Melamed, R., Trejo, A., Ornatsky, O.I., Balderas, R.S., Plevritis, S.K., Sachs, K., Peer, D., Tanner, S.D., Nolan, G.P., 2011. Science 332, 687–696.
Bhardwaj, J., Devarakonda, S., Kumar, S., Jang, J., 2017. Sens. Actuators B Chem. 253, 115–123.
Brangel, P., Sobarzo, A., Parolo, C., Miller, B.S., Howes, P.D., Gelkop, S., Lutwarna, J.J., Dey, J.M., McKendry, R.A., Lobel, L., Stevens, M.M., 2018. ACS Nano 12, 63–73.
Coleman, B., Coarsey, C., Kabir, M.A., Asghar, W., 2019. Sens. Actuators B Chem. 282, 225–231.
Deng, J.Q., Yang, M.Z., Wu, J., Zhang, W., Jiang, X.Y., 2018a. Anal. Chem. 90, 9132–9137.
Deng, X.L., Wang, C., Gao, Y., Li, J.W., Wen, W., Zhang, X.H., Wang, S.F., 2018b. Biosens. Bioelectron. 105, 211–217.
Dong, D.M., Jiao, L.Z., Du, X.F., Zhao, C.J., 2017. Chem. Commun. 53, 4546–4549.
Fan, E.C., Peng, J.X., He, Y., Wu, Y., Ouyang, H., Xu, Z.Q., Fu, Z.F., 2019. Sens. Actuators B Chem. 285, 271–276.
Fu, X.L., Li, G.L., Tian, H.W., Dong, D.M., 2018. RSC Adv. 8, 39635–39640.
Gaudiuso, R., Melikechi, N., Abdel-Salam, Z.A., Harith, M.A., Palleschi, V., Motto-Ros, V., Busser, B., 2019. Spectrochim. Acta B 152, 123–148.
He, H., Liu, B.L., Wen, S.H., Liao, J.Y., Lin, G.G., Zhou, J.J., Jin, D.Y., 2018. Anal. Chem. 90, 12356–12360.
He, Y., Chen, S.L., Huang, L., Wang, Z.W., Wu, Y.N., Fu, F.F., 2019. Anal. Chem. 91,

1171–1177.
Hostetler, M.J., Zhong, C.-J., Yen, B.K.H., Anderegg, J., Gross, S.M., Evans, N.D., Porter, M., Murray, R.W., 1998. J. Am. Chem. Soc. 120, 9396–9397.
Hu, J., Jiang, Y.Z., Tang, M., Wu, L.L., Xie, H.Y., Zhang, Z.L., Pang, D.W., 2019. Anal. Chem. 91, 1178–1184.
Hu, J.Y., Deng, D.Y., Liu, R., Lv, Y., 2018. J. Anal. At. Spectrom. 33, 57–67.
Jaust-Rubio, M., Tomaso, H., El-Shahawi, M.S., Bashammskh, A.S., Al-Youbi, A.O., O'Sullivan, C.K., 2018. Anal. Chem. 90, 12745–12751.
Lai, H.Z., Wang, S.G., Wu, C.Y., Chen, Y.C., 2015. Anal. Chem. 87, 2114–2120.
Liao, W.L., Lin, Q.Y., Xu, Y., Yang, E.L., Duan, Y.X., 2019. Nanoscale 11, 5346–5354.
Loynachan, C.N., Thomas, M.R., Gray, E.R., Richards, D.A., Kim, J., Miller, B.S., Brookes, J.C., Agarwal, S., Chudasama, V., McKendry, R.A., Stevens, M.M., 2018. ACS Nano 12, 279–288.
Markushin, Y., Sivakumar, P., Connolly, D., Melikechi, N., 2015. Anal. Bioanal. Chem. 407, 1849–1855.
Pardede, M., Lie, T.J., Iqbal, J., Bilal, M., Hedwig, R., Ramli, M., Khumaeni, A., Budi, W.S., Idris, N., Abdulmadjud, S.N., Marpaung, A.M., Karnadi, I., Tanra, I., Lie, Z.S., Suyanto, H., Kurniawan, D.P., Kurniawan, K.H., Kagawa, K., Tjia, M.O., 2019. Anal. Chem. 91, 1571–1577.
Pichaandi, J., Zhao, G.Y., Bouzekri, A., Lu, E., Ornatsky, O., Baranov, V., Nitz, M., Winnik, M.A., 2019. Chem. Sci. 10, 2965–2974.
Ren, W., Ballou, D.R., FitzGerald, R., Irudayaraj, J., 2019. Biosens. Bioelectron. 126, 324–331.
Rubab, M., Shahbaz, H.M., Olaimat, A.N., Oh, D.H., 2018. Biosens. Bioelectron. 105, 49–57.
Tran, V., Walkenfort, B., Konig, M., Salehi, M., Schlucker, S., 2019. Angew. Chem. Int. Ed. 58, 442–446.
Verdoot, N., Basso, C.R., Rossi, B.F., Pedrosa, V.A., 2017. Food Chem. 221, 1792–1796.
Wang, S.Q., Deng, W.F., Yang, L., Tan, Y.M., Xie, Q.J., Yao, S.Z., 2017. ACS Appl. Mater. Interfaces 9, 24440–24445.
Yang, M.Z., Liu, Y., Jiang, X.Y., 2019. Chem. Soc. Rev. 48, 850–884.
Yi, R.X., Yang, X.Y., Zhou, R., Li, J.M., Yu, H.W., Hao, Z.Q., Guo, L.B., Li, X.Y., Lu, Y.F., Zeng, X.Y., 2018. Anal. Chem. 90, 7080–7085.
Yu, J.P., Zhang, Y., Li, H., Yang, H., Wei, H.P., 2016. Biosens. Bioelectron. 77, 366–371.
Yuan, K.S., Mei, Q.S., Guo, X.J., Xu, Y.W., Yang, D.T., Sanchez, B.J., Sheng, B.B., Liu, C.S., Hu, Z.W., Yu, G.C., Ma, H.M., Gao, H., Haisch, C., Niessner, R., Jiang, Z.J., Zhou, H.B., 2018. Chem. Sci. 9, 8781–8795.
Zhang, D., Huang, L., Liu, B., Ni, H.B., Sun, L.D., Su, E.B., Chen, H.Y., Gu, Z.Z., Zhao, X.W., 2018. Biosens. Bioelectron. 106, 204–211.